Four sesquiterpene glycosides from loquat (*Eriobotrya japonica*) leaf ameliorates palmitic acid-induced insulin resistance and lipid accumulation in HepG2 Cells via AMPK signaling pathway

Jiawei Li Equal first author, 1 , **Xiaoqin Ding** Equal first author, 1 , **Tunyu Jian** 1 , **Han Lv** 1 , **Lei Zhao** 1 , **Jing Li** 2 , **Yan Liu** 1 , **Bingru Ren** 1 , **Jian Chen** Corresp. 1, 2

1 Institute of Botany, Jiangsu Province and Chinese Academy of Sciences, Nanjing, China

2 Department of Food Science and Technology, College of Light Industry and Food Engineering, Nanjing Forestry University, Nanjing, China

Corresponding Author: Jian Chen
Email address: chenjian80@aliyun.com

Insulin resistance (IR), caused by impaired insulin signal and decreased insulin sensitivity , is generally responsible for the pathophysiology of type 2 diabetes mellitus (T2DM) . Sesquiterpene glycosides (SGs), the exclusive natural products from loquat leaf, have been regarded as potential lead compounds owing to their high efficacy in hypoglycemia and hypolipidemia. Here, we evaluated the beneficial effects of four single SGs isolated from loquat leaf, including SG1, SG2, SG3 and one novel compound SG4 against palmitic acid-induced insulin resistance in HepG2 cells. SG1, SG3 and SG4 could significantly enhance glucose uptake of insulin-resistant HepG2 cells at non-cytotoxic concentration. Meanwhile, Oil Red O stain showed the decrease of both total cholesterol and triglyceride content, suggesting the amelioration of lipid accumulation by SGs in insulin-resistant HepG2 cells. Further investigations found that the expression levels of phosphorylated AMPK, ACC, IRS-1, and Akt were significantly up-regulated after SGs treatment, on the contrary, the expression levels of SREBP-1 and FAS were significantly down-regulated. Notably, AMPK inhibitor Compound C (CC) blocked the regulative effects, while AMPK activator AICAR mimicked the effects of CA in PA-treated insulin-resistant HepG2 cells. In conclusion, SGs (SG4>SG1≈SG3>SG2) improved lipid accumulation in insulin-resistant HepG2 cells through AMPK signaling pathway.

1 **Four sesquiterpene glycosides from loquat (*Eriobotrya japonica*) leaf**

2 **ameliorates palmitic acid-induced insulin resistance and lipid accumulation in**

3 **HepG2 Cells via AMPK signaling pathway**

4 Jiawei Li[1,*], Xiaoqin Ding[1,*], Tunyu Jian[1], Han Lv[1], Lei Zhao[1], Jing Li[2], Yan Liu[1], Bingru Ren[1],

5 Jian Chen[1,2]

6 **Affiliation**

7 [1] Institute of Botany, Jiangsu Province and Chinese Academy of Sciences, Nanjing 210014, China

8 [2] Department of Food Science and Technology, College of Light Industry and Food Engineering,

9 Nanjing Forestry University, Nanjing 210037, China

10 [*]These authors contributed equally to this work.

11 Correspondence: Dr. Jian Chen, chenjian80@aliyun.com

12 Institute of Botany, Jiangsu Province and Chinese Academy of Sciences

13 Nanjing 210014, P. R. China

14 Tel. and fax: +86-25-84347081

15 E-mail address: chenjian80@aliyun.com

22 **Abstract**

23 Insulin resistance (IR), caused by impaired insulin signal and decreased insulin sensitivity, is

24 generally responsible for the pathophysiology of type 2 diabetes mellitus (T2DM). Sesquiterpene

25 glycosides (SGs), the exclusive natural products from loquat leaf, have been regarded as potential

26 lead compounds owing to their high efficacy in hypoglycemia and hypolipidemia. Here, we

27 evaluated the beneficial effects of four single SGs isolated from loquat leaf, including SG1, SG2,

28 SG3 and one novel compound SG4 against palmitic acid-induced insulin resistance in HepG2

29 cells. SG1, SG3 and SG4 could significantly enhance glucose uptake of insulin-resistant HepG2

30 cells at non-cytotoxic concentration. Meanwhile, Oil Red O stain showed the decrease of both total

31 cholesterol and triglyceride content, suggesting the amelioration of lipid accumulation by SGs in

32 insulin-resistant HepG2 cells. Further investigations found that the expression levels of

33 phosphorylated AMPK, ACC, IRS-1, and Akt were significantly up-regulated after SGs treatment,

34 on the contrary, the expression levels of SREBP-1 and FAS were significantly down-regulated.

35 Notably, AMPK inhibitor Compound C (CC) blocked the regulative effects, while AMPK

36 activator AICAR mimicked the effects of CA in PA-treated insulin-resistant HepG2 cells. In

37 conclusion, SGs (SG4>SG1≈SG3>SG2) improved lipid accumulation in insulin-resistant HepG2

38 cells through AMPK signaling pathway.

39 Keywords: Loquat leaf; Sesquiterpene glycosides; Insulin resistance; HepG2 cells; AMPK

40

41 **Introduction**

42   Diabetes mellitus (DM) has become a heterogeneous global epidemic characterized by

43   chronic hyperglycemia associated with impaired lipids metabolism (Motahari-Tabari et al. 2014).

44   Currently, there are 463 million diabetic patients, and the number is estimated to reach 700 million

45   by 2045 (Saeedi et al. 2019). Most of DM patients are affected by type 2 diabetes mellitus (T2DM)

46   which is mainly due to the role of defects with insulin resistance (Fonseca 2009; Jaiswal et al.

47   2017). Insulin resistance is characterized by the weak sensitivity of insulin in peripheral tissues

48   such as skeletal muscle, adipose tissue and liver, resulting hyperglycemia, hyperinsulinemia and

49   dyslipidemia. As the vital organ for metabolic homeostasis and main target organ of insulin action,

50   liver controls the regulation of glucose and lipid metabolism. Hepatic insulin resistance leads to

51   severely dysregulated glucose homeostasis and lipid over-accumulation, which would aggravate

52   hepatic insulin insensitivity(Samuel & Shulman 2012). Therefore, improving hepatic insulin

53   resistance could be an effective strategy in the prevention of T2DM and diabetes-related diseases.

54   AMP-activated protein kinase (AMPK) is an important kinase that has a critical influence on

55   regulating energy metabolism (Herzig & Shaw 2018). Studies have found that AMPK as a key

56   master switch for regulating fatty acid oxidation, triglyceride, lipogenesis, cholesterol synthesis

57   and gluconeogenesis in the liver (Liu et al. 2019).   Activation of AMPK was proved to decrease

58   cholesterol, plasma glucose and triglycerides production in the liver (Hasenour et al. 2013).

59   Phosphorylated AMPK level was down-regulated in the diabetic liver, and activation of AMPK

60   mediated the reverse of metabolic disorders and alleviation of liver function in diabetes mice (Chen

61   et al. 2020; Liu et al. 2019). Thus, AMPK may be an attractive target for insulin resistance in

62   T2DM. With low toxicity and high efficiency, natural products have been used as alternative anti-

63 T2DM agents. Several natural products have been demonstrated to enhance glucose uptake and

64 attenuate insulin resistance via activating AMPK pathway (Mazibuko-Mbeje et al. 2019; Wang et

65 al. 2017; Yan et al. 2018).

66   The fruit tree, loquat (*Eriobotrya japonica*), is a small evergreen arbor and its leaf is an

67 important traditional herbal medicine capable of counteracting inflammation, diabetes, and cancer

68 (Liu et al. 2016). It has been reported that the chemical constituents of loquat leaf included

69 phenolics (Fu et al. 2020), flavonoids (Lu et al. 2009), terpenoids (Zhang et al. 2019), essential

70 oils (Hong et al. 2010), sesquiterpene glycosides (SGs) (Ao et al. 2015) and polysaccharides (Lu

71 et al. 2019). So far, the pharmacological activities of SGs in loquat were mainly manifested as

72 hypoglycemic and anti-nonalcoholic fatty liver disease (NAFLD). Hypoglycemic activity of SGs

73 which was studied in a C57BL/ks-db/db/Ola hereditary diabetic mouse model showed that one of

74 the SGs produced a marked inhibition of glycosuria (De Tommasi et al. 1991).In addition, SG

75 could significantly reduce the blood glucose level of alloxan-diabetic mouse model, while it had

76 no significant effect on normal mice (Chen et al. 2008). Total SGs have been proven to alleviate

77 oxidative stress and NAFLD in high-fat diet induced mouse model and oleic acid induced cell

78 model of NAFLD (Jian et al. 2017; Jian et al. 2018).

79   Our previous investigations on the phytochemistry of loquat leaf led to the discovery of six

80 SGs (Ao et al. 2015; Chen et al. 2008; Zhao et al. 2015). To our knowledge, the influence of SGs

81 on glucose uptake and lipid accumulation in insulin-resistant HepG2 cells have not been

82 investigated. In this study, three known SGs, nerolidol-3-*O*-α-L-rhamnopyranosyl-(1→4)-α-L-

83 rhamnopyranosyl-(1→2)-[α-L-rhamnopyranosyl-(1→6)]-*β*-D-glucopyranoside (SG1) (Chen et al.

84 2008), nerolidol-3-*O*-α-L-rhamnopyranosyl-(1→4)-α-L-rhamnopyranosyl-(1→2)-*β*-D-

85 glucopyranoside (SG2) (De Tommasi et al. 1991) and nerolidol-3-*O*-α-L-rhamnopyranosyl-

86 (1→2)-[*α*-L-rhamnopyranosyl-(1→6)]-*β*-D-glucopyranoside (SG3) (Ao et al. 2015), together with

87 a new compound named as nerolidol-3-O-*α*-L-arabinopyranosyl-(1→4)-*α*-L-rhamnopyranosyl-

88 (1→2)-[*α*-L-rhamnopyranosyl-(1→6)]-*β*-D-glucopyranoside (SG4), were isolated and structural

89 elucidated from loquat leaf. Given the importance of hepatic functions in the pathogenesis of

90 insulin resistance and T2DM, we used a palmitic acid (PA)-induced insulin resistant (IR) model

91 in HepG2 cells to evaluate the efficacy of these four SGs and tried to elucidate the underlying

92 possible molecular mechanism *in vitro*.

93 **Material and Methods**

94 **Plant Material and Reagents**

95   The loquat leaf, collected from Xishan island, in Suzhou city of Jiangsu Province of China,

96 was identified by Prof. Bingru Ren. A voucher specimen (No. 328636) was deposited in the

97 Herbarium of the Institute of Botany, Jiangsu Province and the Chinese Academy of Sciences.

98   SGs (purity ≥ 98%, HPLC) were prepared in our laboratory. Palmitic acid (PA) was purchased

99 from Macklin (Shanghai, China). Fetal bovine serum (FBS) and Dulbecco modified Eagle medium

100 (DMEM) were obtained from Gibco (Carlsbad, CA, USA). AMPK activator AICAR and inhibitor

101 Compound C (CC) were obtained from Beyotime Institute of Biotechnology (Haimen, China) and

102 Selleck (Houston, TX, USA), respectively. The primary antibodies: anti-phospho-IRS-1 (Tyr895)

103 (#3070S), anti-phospho-Akt (#9271), anti-IRS-1 (#2382S), anti-Akt (#9272), anti-β-actin (#4970)

104 were obtained from Cell Signaling Technology (Danvers, MA, USA), anti-phospho-AMPK

105   (T183/172) and anti-AMPK (D168) were purchased from Bioworld (Bloomington, MN, USA),

106   anti-FAS (10624-2-AP) and anti-ACC (21923-1-AP) were   purchased from Proteintech Group

107   (Chicago, USA), and anti-p-ACC (sc-271965) and anti-SREBP-1 (sc-365513) were purchased

108   from Santa Cruz Biotechnology (Santa Cruz, CA, USA). HRP-linked anti-mouse (#7076) and anti-

109   rabbit (#7074) secondary antibodies were obtained from Cell Signaling Technology (Danvers,

110   MA, USA). CCK-8 assay and BCA Protein Quantification Kit were purchased from Biosharp

111   (Hefei, China). Oil Red O stain kit (For Cultured Cells) was obtained from Solarbio (Beijing,

112   China). Total cholesterol (TC), triglyceride (TG) and glycogen assay kits were obtained from

113   Nanjing Jiancheng Bioengineering Institute (Nanjing, China). 2-[N-(7-nitrobenz-2-oxa-1,3-

114   diazol-4-yl) amino]-2-deoxy-D-glucose (2-NBDG) was purchased from Life Technologies

115   (Carlsbad, CA, USA). 10% SDS-PAGE was obtained from EpiZyme Biotechnology (Shanghai,

116   China). Polyvinylidene difluoride membranes were purchased from Millipore (Millipore, MA,

117   USA). High-sig chemiluminescence (ECL) reagent was purchased from Tanon (Shanghai, China).

118   EtOH and the other reagents were obtained from Sinopharm Chemical Reagent Co., Ltd.

119   **Extraction and Isolation**

120   The method for extraction and isolation of SGs were as follows: the dried leaf of loquat (10

121   kg) was pulverized into powder and percolated with 80% EtOH for two months at room

122   temperature. The combined extract was evaporated under reduced pressure to remove alcohol,

123   afterward, the extracts were centrifuged (3000 g for 15 min), and the supernatants were column

124   chromatographed over macroporous resin (XAD16) eluting with 0, 40%, 60%, 70%, and 95%

125   EtOH, respectively. The 60% and 70% EtOH eluted fractions were combined and further column

126   chromatographed over polyamide eluting with different ultrapure H_2O: EtOH mixtures (10:0, 7:3,

127   5:5, 3:7, 0:10), respectively. The H_2O elution fraction was collected and column chromatographed

128   by RP-C18 with H_2O: MeOH mixtures (9:1, 7:3, 5:5, 4:6, 3:7, 8:2, 0:10) as solvent to obtain a total

129   of SGs compounds (1.02 g). The final purification of SG1 (203.0 mg), SG2 (13.8 mg), SG3 (158.6

130   mg) and SG4 (12.4 mg) were achieved by preparative HPLC (LC-6AD, Shimadzu) on a RP-C18

131   column (5 μm, 9.4 × 250 mm, Agilent) with 65~70% MeOH. The NMR spectrum was obtained

132   from a Bruker Avance III 400 MHz spectrometer in DMSO-d_6. HR-ESI-MS spectrum was

133   recorded on a 6530 UPLC-Q-TOF mass spectrometer (Agilent, USA). The acid hydrolysis of SG1-

134   4 and their sugar analysis were carried out as described previously(Ao et al. 2015).

135   **Cell Culture**

136   HepG2 cells were obtained from the Cell Bank of Shanghai Institute of Cell Biology, Chinese

137   Academy of Sciences. The cells were cultured in DMEM supplemented with 10% FBS and 1%

138   antibiotics (penicillin and streptomycin) in a humidified atmosphere with 5% CO_2 at 37 °C.

139   **Cell Counting Kit-8 (CCK-8) Assay**

140   The cell viabilities were assessed using CCK-8 assay. In brief, HepG2 cells were plated into

141   96-well plates with 2×10^5 per well and incubated overnight. Afterwards, the medium was changed

142   with DMEM containing different concentrations of SGs for another 24 h. Subsequently, CCK-8

143   working solution was added to each well and cultivated for another 1 h. The absorbance was

144   recorded on Microplate reader at 450 nm (Molecular Device, Sunnyvale, USA).

145   **Induction of IR HepG2 Cells Model**

146   The IR model was induced in HepG2 cells with 0.25 mM PA (Heo et al. 2018). PA-bovine

147   serum albumin (BSA) conjugate was prepared by dissolving in 50% ethanol and mixing in aqueous

148   BSA solution, and finally diluted in culture media. The cells cultured with BSA only served as the

149   control. HepG2 cells were pre-treated with or without 250 μM PA for 24 h, then incubated in the

150   culture media with or without 250 μM PA or SGs (5 and 10 μM, dissolved in ultrapure water) for

151   another 24 h. Control media was prepared to contain equivalent amount of ethanol and BSA.

152   **Measurement of Glucose Uptake and glycogen content**

153   The uptake of 2-NBDG in HepG2 cells were measured as follows: HepG2 cells were seeded

154   in 96-well plates at a concentration of 2×10^5 per well, then to induce IR and intervened with SGs

155   as described above. Subsequently, the cells were incubated in glucose-free DMEM with 100 nM

156   insulin for 30 min, and then they were incubated with 100 μM 2-NBDG for another 30 min or

157   harvested. The fluorescent intensity was measured on a multimode microplate reader (Berthold

158   TriStar LB941, Germany) at 485 nm excitation and 535 nm emission wavelengths. Harvested cells

159   were used to detect glycogen content according to the manufacturer's instruction.

160   **Measurement of lipid uptake in HepG2 cells**

161   The cells were homogenized in lysis buffer. The levels of intracellular TC and TG were

162   detected with commercial assay kits following the manufacturer's instruction. The data were

163   normalized against protein concentration.

164   The total lipid content in HepG2 cells was measured by Oil red O staining. Briefly, the cells

165   were fixed in 4% formaldehyde for 15 min and then cleaned with PBS, stained with Oil Red O

166   working solution for 30 min. After immediately washed with 60% isopropanol, incubated with

167 hematoxylin for 5 minutes and washed by PBS, the cells were immediately imaged using

168 microscopy (Olympus, Tokyo, Japan), and quantified by ImageJ version 1.52a software ((NIH,

169 USA).

Western Blot Analysis

171   After treatment as above, the total proteins of HepG2 cells were obtained through cell lysis

172 buffer containing 0.1mM of phenylmethanesulfonyl fluoride. Then the cell lysates were

173 centrifuged (12,000 g for 15 min) at 4 °C. Supernatants were prepared and the protein

174 concentration was assayed with BCA Protein Quantification Kit according to the manufactory's

175 instructions. Protein from the samples was separated by SDS-PAGE, transferred to PVDF

176 membranes and then blocked with 5% fat-free milk and incubated at 4 ℃ overnight. The membrane

177 was incubated with primary antibody at 4°C for 24 h, then washed with Tris Buffered saline Tween

178 (TBST) followed by incubating the blot with secondary antibody. Membranes were visualized

179 using the enhanced chemiluminescence (Tanon, China). The band intensities were analyzed using

180 ImageJ version 1.52a software (NIH, USA).

Statistical Analysis

182   The experimental data was performed as the means ± SD. Multiple comparisons were done

183 by One-way analysis of variance (ANOVA) followed by Dunnett's post hoc test using GraphPad

184 Prism 8. Data were considered statistically significant at a P-value of less than 0.05.

Results

Identification of SG4

187   SG4 was obtained as a white powder. It was identified to have a molecular formula of

188    $C_{38}H_{64}O_{18}$ on the basis of the high-resolution electrospray ionization-time of flight mass

189   spectrometry (*m/z* 807.5577 [M-H]$^-$). SG4 was assumed to be a sesquiterpene glycoside since its

190   physicochemical properties and spectral characteristics (**Table 1**). In the ^{1}H NMR spectrum, δ_H

191   5.21 (H-1a, 1H), 5.17 (H-1b, 1H), 5.76 (H-2, 1H), 5.08 (H-6, 1H) and 5.07 (H-10, 1H) could be

192   assigned to a vinyl proton. The proton signals at δ_H 1.56 (H-12, 3H) and 1.63 (H-15, 3H) exhibited

193   a gem-dimethyl group on olefinic carbons. The singlet at δ_H 1.54 (H-14, 3H) indicated a methyl

194   next to a double bond, and the singlet at δ_H 1.27 (H-13, 3H) was deduced to be another methyl

195   group on a quaternary carbon. The four multiple peaks, each integrating two protons at δ_H 1.46 (H-

196   4), 1.92 (H-5), 1.94 (H-8) and 2.01 (H-9), could be inferred from the relevant methylenes. In ^{13}C

197   NMR spectrum, the signals at δ_C 116.1 (C-1), 143.4 (C-2), 124.7 (C-6), 134.7 (C-7), 124.6 (C-10)

198   and 131.1 (C-11) were assigned to three pairs of olefinic carbon signals. The signal at δ_C 80.0

199   (C-3) showed one oxygenated carbon as well. By comparison of values data in previous reference

200   (De Tommasi et al. 1990), it was suggested that the aglycone of SG4 was nerolidol.

201   The downfield shift in the ^{13}C NMR spectrum of SG4 demonstrated that it was glycosylated

202   at the C-3 position. In the sugar portion, four protons at δ_H 4.25 (H-1', 1H), 5.13 (H-1'', 1H), 4.32

203   (H-1''', 1H), and 4.56 (H-1'''', 1H) in ^{1}H NMR spectrum were examined to be correlated with their

204   sugar anomeric carbons at δ_C 96.9 (C-1'), 100.2 (C-1''), 106.2 (C-1''') and 101.3 (C-1'''') in HMQC

205   spectrum, respectively. According to pre-column derivatization GC analysis of authentic

206   monosaccharides, the monosaccharides of SG4 were determined to be D-glucose, L-rhamnose and

207   L-arabinose (ratio1:2:1). The signal at $J_{H-1', H-2'}$ (7.6 Hz) indicated that the β-anomeric configuration

208   of the glucose, and the resonances of C-3 (δ_C 71.0, 71.1) and C-5 (δ_C 66.8, 68.8) demonstrated that

209   the α-anomeric configurations of the rhamnose units, and the signal at $J_{\text{H-1'''},\text{ H-2'''}}$ (7.5 Hz) suggested

210   that the α-anomeric configuration of arabinose (Kasai et al. 1979). HMBC spectrum correlations

211   showed that the following sequence of the sugar linkages connected to the aglycone: H-1'' (δ_H

212   5.13) of rhamnose I with C-2' (δ_C 78.5) of glucose, H-1''' (δ_H 4.32) of arabinose with C-4'' (δ_C 83.7)

213   of rhamnose I H-1' (δ_H 4.25) of glucose with C-3 (δ_C 80.0) of aglycone, and H-1'''' (δ_H 4.56) of

214   rhamnose II with C-6' (δ_C 67.5) of glucose (**Table 1**). Therefore, SG4 was analyzed to be one new

215   compound, and it was characterized as nerolidol-3-O-α-L-arabinopyranosyl-(1→4)-α-L-

216   rhamnopyranosyl-(1→2)-[α-L-rhamnopyranosyl-(1→6)]-β-D-glucopyranoside (**Figure 1**).

217   **The Effects of SGs on HepG2 Cells Viability**

218   The cytotoxic effect of a series concentration of SGs (50-250 μM) in HepG2 cells was

219   evaluated using CCK-8 assay after 24 h incubation. As shown in **Figure 2**, the viability of cells

220   treated with 250 μM of SG1, 200 μM and 250 μM of SG2 were all significantly reduced,

221   accordingly, both SG3 and SG4 at concentration of 250 μM significantly reduced cells viability as

222   well. These results showed that SGs displayed distinct growth inhibition when drug concentrations

223   were more than 200 or 250 μM, indicating that 5 or 10 μM concentrations of SGs for the present

224   study were safe on HepG2 cells.

225   **The Effects of SGs on Glucose uptake and glycogen content in IR HepG2 Cells**

226   Studies pointed out that glucose uptake assay in IR cells determined whether compounds

227   could ameliorate IR in HepG2 cells induced by PA (Tong et al. 2018). As shown in **Figure 3A**

228   **and B**, both the glucose uptake and glycogen content of IR group were significantly lower than

229   that of control group after 24 h treatments. On the contrary, a remarkable increase of glucose

230   uptake and glycogen content were detected in SGs-treated group (except for SG2) in comparison

231   with the IR group.

232   **The Effects of SGs on Lipid Accumulation in IR HepG2 Cells**

233   The Oil Red O stain method was used to evaluate lipid accumulation in insulin-resistant

234   HepG2 cells. As shown in **Figure 3B**, compared with control group, insulin-resistant HepG2 cells

235   had much more lipid droplets, while the SGs-treatments (except for SG2) caused a significant

236   decrease in lipid droplets. These results were further confirmed by the contents of TC and TG in

237   the cells. As shown in **Figure 3C** and **D**, in comparison with control group, the level of TC and

238   TG increased significantly after PA inducing, on the contrary, the SGs-treated groups caused a

239   significant decrease.

240   **The Effects of SGs on AMPK Signaling Pathways in IR HepG2 Cells**

241   To investigate underlying possible molecular mechanism of SGs ameliorating lipid

242   accumulation and IR in PA-induced HepG2 cells, we investigated the effects of SGs on the protein

243   expression of the AMPK pathway. As shown in **Figure 4**, in comparison with control group, PA-

244   treatment significantly decreased the phosphorylation levels of AMPK, ACC, IRS1 and Akt, and

245   up-regulated SREPB-1 and FAS protein level. However, in comparison with IR group,

246   phosphorylation levels of AMPK, ACC, IRS-1 and Akt were significantly up-regulated in SGs-

247   treated groups, especially in high concentration (10 μM) of SG4, while SG2 had no significant

248   effects on the expressions of p-Akt and p-IRS-1. Moreover, in comparison with IR group, SGs-

249   treated groups (except for SG2) showed a significant reduction of SREBP-1 and FAS level.

250   To confirm whether SGs regulates AMPK to activate IRS1/Akt insulin signal pathway and

251   decrease SREBP-1/FAS pathway, AMPK activator AICAR and AMPK inhibitor compound C

252   were used in PA-treated HepG2 cells. The results showed that AICAR (0.5 mM) up-regulated

253   phosphorylation levels of ACC and IRS1, and reduced SREBP-1 protein level in PA-treated

254   HepG2 cells. However, CC (10 μM) partly abolished, the up-regulative effect of SGs on

255   phosphorylation levels of ACC and IRS1, and the down-regulative effect of SGs on SREBP-1

256   protein level (Figure 5). These results suggested that AMPK pathway was involved in the SGs-

257   mediated IRS1 and SREBP-1 pathways in PA-treated HepG2 cells.

258   **Discussion**

259   As an important traditional Chinese medicine, loquat leaf has been widely used with

260   beneficial effects in numerous diseases including chronic bronchitis, asthma and diabetes (Fu et

261   al. 2019; Kim et al. 2020; Li et al. 2004; Zhang et al. 2019). Our previous study has confirmed the

262   alleviation of hepatic lipid accumulation and hyperlipidemia of total SGs from loquat leaves in

263   high-fat diet induced NAFLD mouse model. In this work, we revealed the improvement of insulin

264   resistance and lipid accumulation of four individual SGs from loquat leaves, including three known

265   SGs (SG1, SG2, SG3) (Ao et al. 2015; Chen et al. 2008) and one new compound SG4.

266   Furthermore, possible cellular mechanism of SGs on the amelioration of lipid-induced IR was

267   elucidated by exploring downstream signal pathways involved in AMPK-mediated pathway.

268   It is well known that IR is the main mechanism of T2DM pathogenesis. Liver is a critical

269   metabolic organ in maintenance of glucose and lipid homeostasis (Birkenfeld & Shulman 2014).

270   It has been shown that excessive nutrients induce a greater increase in liver fat and insulin

271   resistance and long-term treatment with PA can cause IR (Malik et al. 2019). PA-induced cells

272   have been widely used as an IR model *in vitro*. In the present study, we used 0.25 mM PA to

273   induce IR in HepG2 cells. The CCK-8 assay showed that 5 μM or 10 μM SGs were safe in IR

274   HepG2 cells. Further, we found that SGs significantly enhanced glucose uptake in PA-induced IR

275   HepG2 cells. On the other hand, SGs administration established a significant decrease of lipid

276   deposition in PA-induced HepG2 cells, as well as down-regulated intracellular TC and TG levels

277   at a low concentration.

278   AMPK, an energy sensor, is believed to systematically adjust the lipid metabolism balance,

279   including the regulation of plasma glucose levels, fatty acid oxidation and glycogen metabolism.

280   Several evidences indicated that activation of AMPK is an effective approach for improving

281   insulin sensitivity by stimulating glucose uptake (Fryer & Carling 2005). In the liver, AMPK

282   activation promotes glucose uptake and suppresses lipid and cholesterol synthesis (Yan et al.

283   2018). Acetyl-CoA carboxylase (ACC) is a key substrate of AMPK (Cesquini et al. 2008). Once

284   activated, AMPK modulates insulin signaling through the phosphorylation of key proteins that

285   promotes insulin responsiveness, including IRS and Akt. The dysregulation of IRS is a common

286   underlying mechanism in IR (DeFronzo & Tripathy 2009; Karlsson & Zierath 2007). Among

287   isoforms of IRS, IRS-1 is more closely related to glucose homeostasis. Two forms of

288   phosphorylation of IRS-1, serine phosphorylation and tyrosine phosphorylation, coordinately

289   regulate insulin signaling. It has been reported that the serine phosphorylation of IRS-1 protects

290   IRS-1 from the tyrosine phosphorylation under insulin stimulation (Gual et al. 2005). In addition,

291   the serine phosphorylation of IRS-1 inhibits Akt activity under obese conditions and then impairs

292   IRS-1/PI3K/Akt signal pathways (Gao et al. 2002). Hence, we investigated the effects of SGs on

293   the expression of the target genes associated with insulin signal pathways. In this study, PA

294   reduced the phosphorylation expression of AMPK, ACC, IRS-1 and Akt. In consist with the up-

295   regulation of glucose uptake, SGs reversed the phosphorylation expression of AMPK, IRS-1 and

296   Akt in PA-induced IR HepG2 cells. PA-induced decrease of ACC and IRS1 phosphorylation was

297   reversed by AICAR. Importantly, SGs mediated up-regulative effect on ACC and IRS1

298   phosphorylation was partly eliminated by CC. These results demonstrated that SGs could

299   ameliorated insulin resistance through AMPK/IRS-1/Akt pathway.

300   Sterol regulatory element binding proteins (SREBPs), are key lipogenic transcription factors

301   regulating cellular lipid metabolism and modulated by glucose and insulin (Ruiz et al. 2014; Zhu

302   et al. 2019). Among isoforms of SREBPs, SREBP-1 is essential to control expression of enzymes

303   of carbohydrate and fatty acid metabolism (Hua et al. 2016). It was well-documented that SREBP-

304   1 positively regulated the expression of genes encoding lipogenic enzymes including fatty acid

305   synthase (FAS) (Shimano 2001). As a cellular energy sensor, AMPK signaling is regarded as one

306   of the most important regulators of lipid homeostasis (Hardie et al. 2012). On the upstream of

307   SREBP-1, AMPK could suppress SREBP-1 mediated lipogenesis (Li et al. 2011). As expected, in

308   consist with the down-regulation of intracellular TC and TG levels and the alleviation of lipid

309   deposition, SGs down-regulated SREBP-1 and FAS protein level in PA-induced IR HepG2 cells.

310   In addition, AICAR reversed PA-induced SREBP-1 elevation, while CC partly abolished SGs

311   mediated SREBP-1 reduction. These results demonstrated that SGs repressed the lipogenesis in IR

312   HepG2 cells via the AMPK/SREBP-1/FAS pathway.

313   Noticeably, SG4 was the most prominent compound when comparing to other SGs, while

314   SG2 had no significant effect on insulin resistance improvement. Compared with SG1, SG3 had a

315   similar therapeutic effect. By comparison of structure-activity relationship, we found that SGs

316   were composed of nerolidol as aglycone and oligosaccharide chain. It is suggesting that the

317   oligosaccharide chain part influences the effect, and the difference among them occurs because of

318   the saccharide category and the amount of saccharide. Compared with SG1, SG2 lacks one

319   rhamnose on the junction with glucose C-6, while SG3 lacks the other rhamnose on the junction

320   with rhamnose C-4 which is connected to glucose C-2. However, one rhamnose at the end of the

321   oligosaccharide chain is replaced by arabinose in SG4. Based on the above analysis, we speculate

322   that the number of saccharides in SGs unit has a significant effect on activities. Moreover, both

323   C-6 of glucose and C-4 of rhamnose are potential active sites, which need to be further

324   investigated.

325   **Conclusions**

326   In summary, we stated a new sesquiterpene glycoside (SG4), namely as nerolidol-3-O-α-L-

327   arabinopyranosyl-(1→4)-α-L-rhamnopyranosyl-(1→2)-[α-L-rhamnopyran-osyl-(1→6)]-β-D-

328   glucopyranoside, which was isolated in loquat leaf for the first time. Interestingly, our further

329   research demonstrated that SG4, like other SGs from loquat leaf, could promote glucose uptake

330   and ameliorate lipid accumulation in PA-induced insulin-resistant HepG2 cells. SGs may act as

331   potential natural products regulating glucose and lipid metabolism in T2DM. The potential

332   mechanism might be associated with the activation of AMPK/IRS-1/Akt pathway and inhibition

333   of SREBP-1/FAS pathway.

334 ADDITIONAL INFORMATION AND DECLARATIONS

335 **Funding**

336 The authors are indebted to the research grants from the National Natural Science Foundation of

337 China (No.81773885; No.81703224; No.31770366; No.81973463) and Jiangsu Scientific and

338 Technological Innovations Platform (Jiangsu Provincial Service Center for Antidiabetic Drug

339 Screening). Thanks to the support of Jiangsu Key Laboratory for the Research and Utilization of

340 Plant Resources.

341 **Competing Interests**

342 The authors declare that they have no conflict of interest.

343 **Author Contributions**

344 Design of the study: JC, XQD and TYJ; plants collection: BRR and YL; extraction and separation

345 of SGs: HL, LZ; data collection and analysis: JWL, JL; analysis and interpretation of the data:

346 TYJ, JWL; drafting the manuscript: JWL; critical revision of the manuscript: JC, XQD.

347 **Animal Ethics**

348 The authors declare that no experiments were performed on humans or animals for this study.

349 **Data Availability**

350 The following information was supplied regarding data availability:

351 The raw data are available as Supplemental Files.

352 **References**

353 **Ao XC, Zhao L, Lv H, Ren BR, Wu H, Chen J, and Li WL. 2015.** New Sesquiterpene Glycosides from the Leaves

354 of *Eriobotrya japonica. Natural Product Communications* 10:1145-1147. doi:

355   10.1177/1934578X1501000702.

356   **Birkenfeld AL, and Shulman GI. 2014.** Nonalcoholic fatty liver disease, hepatic insulin resistance, and type 2

357   diabetes. *Hepatology* 59:713-723. doi: 10.1002/hep.26672.

358   **Cesquini M, Stoppa GR, Prada PO, Torsoni AS, Romanatto T, Souza A, Saad MJ, Velloso LA, and Torsoni**

359   **MA. 2008.** Citrate diminishes hypothalamic acetyl-CoA carboxylase phosphorylation and modulates satiety

360   signals and hepatic mechanisms involved in glucose homeostasis in rats. *Life Sciences* 82:1262-

361   1271.10.1016/j.lfs.2008.04.015.

362   **Chen J, Li WL, Wu JL, Ren BR, and Zhang HQ. 2008.** Hypoglycemic effects of a sesquiterpene glycoside isolated

363   from leaves of loquat (*Eriobotrya japonica (Thunb.) Lindl.*). *Phytomedicine* 15:98-102. doi:

364   10.1016/j.phymed.2006.12.014.

365   **Chen L, Lin X, Fan X, Qian Y, Lv Q, and Teng H. 2020.** Sonchus oleraceus Linn extract enhanced glucose

366   homeostasis through the AMPK/Akt/ GSK-3beta signaling pathway in diabetic liver and HepG2 cell culture.

367   *Food and Chemical Toxicology* 136:111072. doi: 10.1016/j.fct.2019.111072.

368   **De Tommasi N, De Simone F, Cirino G, Cicala C, and Pizza C. 1991.** Hypoglycemic effects of sesquiterpene

369   glycosides and polyhydroxylated triterpenoids of *Eriobotrya japonica*. *Planta Medica* 57:414-416. doi:

370   10.1055/s-2006-960137.

371   **DeFronzo RA, and Tripathy D. 2009.** Skeletal muscle insulin resistance is the primary defect in type 2 diabetes.

372   *Diabetes Care* 32 Suppl 2:S157-163.doi: 10.2337/dc09-S302.

373   **Fonseca VA. 2009.** Defining and characterizing the progression of type 2 diabetes. *Diabetes Care* 32 Suppl 2:S151-

374   156. doi:10.2337/dc09-S301.

375   **Fryer LG, and Carling D. 2005.** AMP-activated protein kinase and the metabolic syndrome. *Biochemical Society*

376   *Transactions* 33:362-366. doi: 10.1042/BST0330362.

377   **Fu Y, Li F, Ding Y, Li HY, Xiang XR, Ye Q, Zhang J, Zhao L, Qin W, Gan RY, and Wu DT. 2020.**

378   Polysaccharides from loquat (*Eriobotrya japonica*) leaves: Impacts of extraction methods on their

379   physicochemical characteristics and biological activities. *International Journal of Biological*

380   *Macromolecules* 146:508-517. doi: 10.1016/j.ijbiomac.2019.12.273.

381   **Fu Y, Yuan Q, Lin S, Liu W, Du G, Zhao L, Zhang Q, Lin DR, Liu YT, Qin W, Li DQ, and Wu DT. 2019.**

382   Physicochemical characteristics and biological activities of polysaccharides from the leaves of different

383   loquat (*Eriobotrya japonica*) cultivars. *International Journal of Biological Macromolecules* 135:274-281.

384   doi: 10.1016/j.ijbiomac.2019.05.157.

385   **Gao Z, Hwang D, Bataille F, Lefevre M, York D, Quon MJ, and Ye J. 2002.** Serine phosphorylation of insulin

386   receptor substrate 1 by inhibitor kappa B kinase complex. *Journal of Biological Chemistry* 277:48115-48121.

387   doi: 10.1074/jbc.M209459200.

388   **Gual P, Le Marchand-Brustel Y, and Tanti JF. 2005.** Positive and negative regulation of insulin signaling through

389   IRS-1 phosphorylation. *Biochimie* 87:99-109. doi: 10.1016/j.biochi.2004.10.019.

390   **Hardie DG, Ross FA, and Hawley SA. 2012.** AMPK: a nutrient and energy sensor that maintains energy

391   homeostasis. *Nature Reviews: Molecular Cell Biology* 13:251-262. doi: 10.1038/nrm3311.

392   **Hasenour CM, Berglund ED, and Wasserman DH. 2013.** Emerging role of AMP-activated protein kinase in

393   endocrine control of metabolism in the liver. *Molecular and Cellular Endocrinology* 366:152-162. doi:

394   10.1016/j.mce.2012.06.018.

395   **Heo JI, Yoon DW, Yu JH, Kim NH, Yoo HJ, Seo JA, Kim SG, Choi KM, Baik SH, Choi DS, and Kim NH.**

396   **2018.** Melatonin improves insulin resistance and hepatic steatosis through attenuation of alpha-2-HS-

397   glycoprotein. *Journal of Pineal Research* 65:e12493. doi:10.1111/jpi.12493.

398   **Herzig S, and Shaw RJ. 2018.** AMPK: guardian of metabolism and mitochondrial homeostasis. *Nature Reviews:*

399   *Molecular Cell Biology* 19:121-135. doi: 10.1038/nrm.2017.95.

400   **Hong Y, SH H, JC W, and SQ L. 2010.** Identification of essential oils from the leaves of 11 species of *Eriobotrya*.

401   *Pak J Bot* 42:4379-4386.

402   **Hua S, Li Y, Su L, and Liu X. 2016.** Diosgenin ameliorates gestational diabetes through inhibition of sterol regulatory

403   element-binding   protein-1.   *Biomedicine   and   Pharmacotherapy*   84:1460-1465.   doi:

404   10.1016/j.biopha.2016.10.049.

405   **Jaiswal M, Divers J, Dabelea D, Isom S, Bell RA, Martin CL, Pettitt DJ, Saydah S, Pihoker C, Standiford DA,**

406   **Dolan LM, Marcovina S, Linder B, Liese AD, Pop-Busui R, and Feldman EL. 2017.** Prevalence of and

407   Risk Factors for Diabetic Peripheral Neuropathy in Youth With Type 1 and Type 2 Diabetes: SEARCH for

408   Diabetes in Youth Study. *Diabetes Care* 40:1226-1232. Doi: 10.2337/dc17-0179.

409   **Jian T, Ao X, Wu Y, Lv H, Ma L, Zhao L, Tong B, Ren B, Chen J, and Li W. 2017.** Total sesquiterpene glycosides

410   from Loquat (*Eriobotrya japonica*) leaf alleviate high-fat diet induced non-alcoholic fatty liver disease

411   through cytochrome P450 2E1 inhibition. *Biomedicine and Pharmacotherapy* 91:229-237. doi:

412   10.1016/j.biopha.2017.04.056.

413   **Jian T, Wu Y, Ding X, Lv H, Ma L, Zuo Y, Ren B, Zhao L, Tong B, Chen J, and Li W. 2018.** A novel

414   sesquiterpene glycoside from loquat leaf alleviates oleic acid-induced steatosis and oxidative stress in HepG2

415   cells. *Biomedicine and Pharmacotherapy* 97:1125-1130. doi: 10.1016/j.biopha.2017.11.043.

416   **Karlsson HK, and Zierath JR. 2007.** Insulin signaling and glucose transport in insulin resistant human skeletal

417   muscle. *Cell Biochemistry and Biophysics* 48:103-113. doi: 10.1007/s12013-007-0030-9.

418   **Kim TM, Paudel KR, and Kim DW. 2020.** *Eriobotrya japonica* leaf extract attenuates airway inflammation in

419   ovalbumin-induced mice model of asthma. *Journal of Ethnopharmacology* 253:112082. doi:

420   10.1016/j.jep.2019.112082.

421   **Li WL, Zheng HC, Bukuru J, and De Kimpe N. 2004.** Natural medicines used in the traditional Chinese medical

422   system for therapy of diabetes mellitus. *Journal of Ethnopharmacology* 92:1-21.10.1016/j.jep.2003.12.031

423   **Li Y, Xu S, Mihaylova MM, Zheng B, Hou X, Jiang B, Park O, Luo Z, Lefai E, Shyy JY, Gao B, Wierzbicki M,**

424   **Verbeuren TJ, Shaw RJ, Cohen RA, and Zang M. 2011.** AMPK phosphorylates and inhibits SREBP

425   activity to attenuate hepatic steatosis and atherosclerosis in diet-induced insulin-resistant mice. *Cell Metab*

426   13:376-388. doi: 10.1016/j.cmet.2011.03.009.

427   **Liu Y, Deng J, and Fan D. 2019.** Ginsenoside Rk3 ameliorates high-fat-diet/streptozocin induced type 2 diabetes

428   mellitus in mice via the AMPK/Akt signaling pathway. *Food Funct* 10:2538-2551. doi: 10.1039/c9fo00095j.

429   **Liu Y, Zhang W, Xu C, and Li X. 2016.** Biological Activities of Extracts from Loquat (*Eriobotrya japonica Lindl.*):

430   A Review. *Int J Mol Sci* 17(12): 1983. Doi: 10.3390/ijms17121983.

431   **Lv H, Chen J, Li WL, Ren BR, Wu JL, and Zhang HQ. 2009.** Hypoglycemic effect of the total flavonoid fraction

432   from *folium Eriobotryae*. *Phytomedicine* 16:967-971. doi: 10.1016/j.phymed.2009.03.024.

433   **Lu T, Fan Z, Hou J, Qi X, Guo M, Ju J, Yang Y, and Gu C. 2019.** Loquat leaf polysaccharides improve glomerular

434   injury in rats with anti-Thy 1 nephritis via peroxisome proliferator-activated receptor alpha pathway. *Am J*

435   *Transl Res* 11:3531-3542

436 **Malik SA, Acharya JD, Mehendale NK, Kamat SS, and Ghaskadbi SS. 2019.** Pterostilbene reverses palmitic acid

437   mediated insulin resistance in HepG2 cells by reducing oxidative stress and triglyceride accumulation. *Free*

438   *Radical Research* 53:815-827. doi: 10.1080/10715762.2019.1635252.

439 **Mazibuko-Mbeje SE, Dludla PV, Roux C, Johnson R, Ghoor S, Joubert E, Louw J, Opoku AR, and Muller**

440   **CJF. 2019.** Aspalathin-Enriched Green Rooibos Extract Reduces Hepatic Insulin Resistance by Modulating

441   PI3K/AKT and AMPK Pathways. *Int J Mol Sci* 20(3):633. doi: 10.3390/ijms20030633.

442 **Motahari-Tabari N, Ahmad Shirvani M, Shirzad EAM, Yousefi-Abdolmaleki E, and Teimourzadeh M. 2014.**

443   The effect of 8 weeks aerobic exercise on insulin resistance in type 2 diabetes: a randomized clinical trial.

444   *Glob J Health Sci* 7:115-121. doi: 10.5539/gjhs.v7n1p115.

445 **Ruiz R, Jideonwo V, Ahn M, Surendran S, Tagliabracci VS, Hou Y, Gamble A, Kerner J, Irimia-Dominguez**

446   **JM, Puchowicz MA, DePaoli-Roach A, Hoppel C, Roach P, and Morral N. 2014.** Sterol regulatory

447   element-binding protein-1 (SREBP-1) is required to regulate glycogen synthesis and gluconeogenic gene

448   expression in mouse liver. *Journal of Biological Chemistry* 289:5510-5517. doi: 10.1074/jbc.M113.541110.

449 **Saeedi P, Petersohn I, Salpea P, Malanda B, Karuranga S, Unwin N, Colagiuri S, Guariguata L, Motala AA,**

450   **Ogurtsova K, Shaw JE, Bright D, Williams R, and Committee IDFDA. 2019.** Global and regional

451   diabetes prevalence estimates for 2019 and projections for 2030 and 2045: Results from the International

452   Diabetes Federation Diabetes Atlas, 9(th) edition. *Diabetes Research and Clinical Practice* 157:107843. doi:

453   10.1016/j.diabres.2019.107843.

454 **Samuel VT, and Shulman GI. 2012.** Mechanisms for insulin resistance: common threads and missing links. *Cell*

455   148:852-871. doi: 10.1016/j.cell.2012.02.017.

456 **Shimano H. 2001.** Sterol regulatory element-binding proteins (SREBPs): transcriptional regulators of lipid synthetic

457   genes. *Progress in Lipid Research* 40:439-452.10.1016/s0163-7827(01)00010-8.

458 **Tong T, Ren N, Soomi P, Wu J, Guo N, Kang H, Kim E, Wu Y, He P, Tu Y, and Li B. 2018.** Theaflavins Improve

459   Insulin Sensitivity through Regulating Mitochondrial Biosynthesis in Palmitic Acid-Induced HepG2 Cells.

460   *Molecules* 23(12):3382. doi: 10.3390/molecules23123382.

461 **Wang T, Jiang H, Cao S, Chen Q, Cui M, Wang Z, Li D, Zhou J, Wang T, Qiu F, and Kang N. 2017.** Baicalin

462   and its metabolites suppresses gluconeogenesis through activation of AMPK or AKT in insulin resistant

463   HepG-2 cells. *European Journal of Medical Chemistry* 141:92-100. doi: 10.1016/j.ejmech.2017.09.049.

464   **Yan J, Wang C, Jin Y, Meng Q, Liu Q, Liu Z, Liu K, and Sun H. 2018.** Catalpol ameliorates hepatic insulin

465   resistance in type 2 diabetes through acting on AMPK/NOX4/PI3K/AKT pathway. *Pharmacological*

466   *Research* 130:466-480. doi: 10.1016/j.phrs.2017.12.026.

467   **Zhang J, Xu HY, Wu YJ, Zhang X, Zhang LQ, and Li YM. 2019.** Neutrophil elastase inhibitory effects of

468   pentacyclic triterpenoids from *Eriobotrya japonica* (loquat leaves). *Journal of Ethnopharmacology*

469   242:111713. doi: 10.1016/j.jep.2019.01.037.

470   **Zhao L, Chen J, Lv H, Ao XC, Ren BR, and Li WL. 2015.** A New Sesquiterpene Glycoside from the Leaves of

471   *Eriobotrya japonica*. *Chemistry of Natural Compounds* 51:1103-1106.

472   **Zhu L, Du W, Liu Y, Cheng M, Wang X, Zhang C, Lv X, Li F, Zhao S, and Hao J. 2019.** Prolonged high-

473   glucose exposure decreased SREBP-1/FASN/ACC in Schwann cells of diabetic mice via blocking

474   PI3K/Akt pathway. *Journal of Cellular Biochemistry* 120:5777-5789. doi: 10.1002/jcb.27864.

475

476 **Table 1.** ^{1}H and ^{13}C NMR Data of SG4 (DMSO-d$_6$, δ, ppm, J/Hz).

477 **Figure 1.** Chemical structures of SGs. (A) SG1: R$_1$ = Rha (1→4) Rha, R$_2$ = Rha; SG2: R$_1$ = Rha

478 (1→4) Rha, R$_2$ = H; SG3: R$_1$ = Rha, R$_2$ = Rha; (B) Chemical structure of SG4* ($_*$ as a novel

479 compound).

480 **Figure 2.** Influence of SGs on cell viability in HepG2 cells. (A, B, C and D) Cell viability of

481 HepG2 cells in different concentrations of SG1, SG2, SG3 and SG4 from 0 to 250 μM ($n = 8$). $^\#P$

482 < 0.05, $^{\#\#}P < 0.01$, $^{\#\#\#}P < 0.001$ compared with the control HepG2 cells.

483 **Figure 3.** SGs on insulin-stimulated glucose uptake and lipid deposition in PA-treated HepG2

484 cells. (A) Glucose uptake in HepG2 cells measured by 2-NBDG method ($n = 8$); (B) Oil Red O

485 stain of HepG2 cells; (C and D) SGs treatment decreased TC and TG content in PA-treated HepG2

486 cells ($n = 8$). $^{\#\#}P < 0.01$, $^{\#\#\#}P < 0.001$ compared with control group; $^*P < 0.05$, $^{**}P < 0.01$, $^{***}P <$

487 0.001 compared with IR group.

488 **Figure 4.** Western blot analysis of protein expression levels of AMPK signaling pathway. (A)

489 Expression strips of all protein; (B) Phosphorylation level of AMPK normalized by AMPK,

490 phosphorylation level of ACC normalized by ACC and phosphorylation level of IRS-1 normalized

491 by IRS-1 ($n = 3$); (C) Phosphorylation level of Akt normalized by Akt ($n = 3$), SREBP-1 and FAS

492 protein levels normalized by β-actin ($n = 3$). $^{\#\#}P < 0.01$ and $^{\#\#\#}P < 0.001$ compared with control

493 group; $^*P < 0.05$, $^{**}P < 0.01$, $^{***}P < 0.001$ compared with IR group.

494 **Figure 5.** Western blot analysis of protein expression levels of AMPK signaling pathway after

495 AICAR and CC treatment. (A) Expression strips of the proteins of p-IRS1, IRS1, SREBP-1 and

496 β-actin; (B) phosphorylation level of ACC normalized by ACC, phosphorylation level of IRS-1

497   normalized by IRS-1 and SREBP-1 protein level normalized by β-actin (n = 3) in HepG2 cells

498   after AICAR treatment; (C) Expression strips of the proteins of p-ACC, ACC, p-IRS1, IRS1,

499   SREBP-1 and β-actin; (D) phosphorylation level of ACC normalized by ACC, phosphorylation

500   level of IRS-1 normalized by IRS-1 and SREBP-1 protein level normalized by β-actin (n = 3) in

501   HepG2 cells after SGs and AICAR treatment. [###]P< 0.001 compared with control group; [*]P< 0.05,

502   [**]$P < 0.01$, [***]$P < 0.001$ compared with IR group.

503

504

^{1}H and ^{13}C NMR Data of SG4

^{1}H and ^{13}C NMR Data of SG4 (DMSO-d$_6$, δ, ppm, J/Hz).

1 **Table 1.** ^{1}H and ^{13}C NMR Data of SG4 (DMSO-d$_6$, δ, ppm, J/Hz)

C atom	δ_C	δ_H	HMBC		C atom	δ_C	δ_H	HMBC
1	116.1	5.21 (1H) 5.17 (1H)	C-3, C-2	Glc	1'	96.9	4.25 (1H, d, J = 7.6 Hz)	C-3
2	143.4	5.76 (1H, dd, J = 17.0, 10.0 Hz)	C-13		2'	78.5	3.28	C-3'
3	80.0				3'	76.3	3.17	C-2', C-1", C-1'
4	41.6	1.46 (m, 2H)	C-3, C-13		4'	69.9	3.26	C-3'
5	22.5	1.92 (m, 2H)	C-6, C-4, C-7		5'	75.6	3.12	
6	124.7	5.08 (submerged, 1H)			6'	67.5	3.77 (1H, m), 3.33 (1H, m)	C-1""
7	134.7			Rha I	1"	100.2	5.13 (brs, 1H)	C-5", C-2", C-3'
8	39.7	1.94 (m, 2H)	C-7, C-9, C-14, C-6		2"	71.2	3.40	C-3"
9	26.7	2.01 (m, 2H)	C-11, C-10, C-8, C-7		3"	71.0	3.59	C-2"
10	124.6	5.07 (submerged, 1H)	C-8, C-9, C-12, C-15		4"	83.7	3.37	C-6", C-1"', C-5", C-3"
11	131.1				5"	66.8	4.00	C-4"
12	18.0	1.56 (s, 3H)	C-11, C-10, C-15		6"	18.0	1.13 (d, J = 6.1 Hz)	C-4", C-5"
13	22.3	1.27 (s, 3H)	C-2, C-3, C-4	Ara	1"'	106.2	4.32 (d, J = 7.5 Hz, 1H)	C-4"
14	16.2	1.54 (s, 3H)	C-7, C-6, C-8		2"'	77.1	3.10	C-3"
15	25.9	1.63 (s, 3H)	C-11, C-10, C-12		3"'	75.0	2.99	C-1"'
					4"'	70.4	3.67	
					5"'	66.5	3.68, 3.03	C-1"'
				Rha II	1""	101.3	4.56 (s, 1H)	C-2"", C-5""
					2""	71.2	3.40	C-3""
					3""	71.1	2.96	
					4""	72.5	3.18	C-6"", C-3"", C-2""
					5""	68.8	3.41	C-4""
					6""	18.4	1.13 (d, J = 6.1 Hz, 3H)	C-5"", C-4""

Figure 1

Chemical structures of SGs

Chemical structures of SGs. (A) SG1: R_1 = Rha (1→4) Rha, R_2 = Rha; SG2: R_1 = Rha (1→4) Rha, R_2 = H; SG3: R_1 = Rha, R_2 = Rha; (B) Chemical structure of SG4* (* as a novel compound).
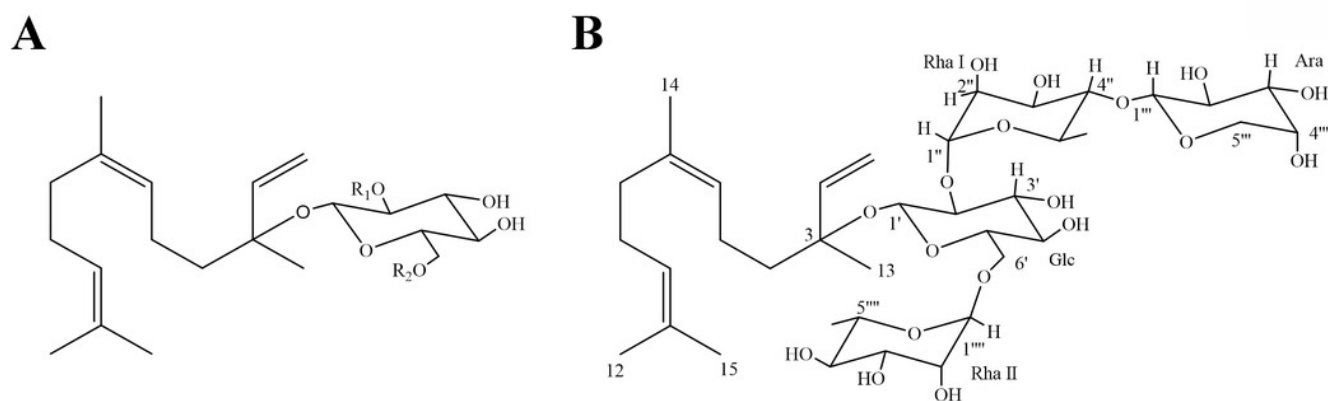
Figure 2

Influence of SGs on cell viability in HepG2 cells

Influence of SGs on cell viability in HepG2 cells. (A, B, C and D) Cell viability of HepG2 cells in different concentrations of SG1, SG2, SG3 and SG4 from 0 to 250 μM (n = 8). $^{#}P$ < 0.05, $^{##}P$ < 0.01, $^{###}P$ < 0.001 compared with the control HepG2 cells.
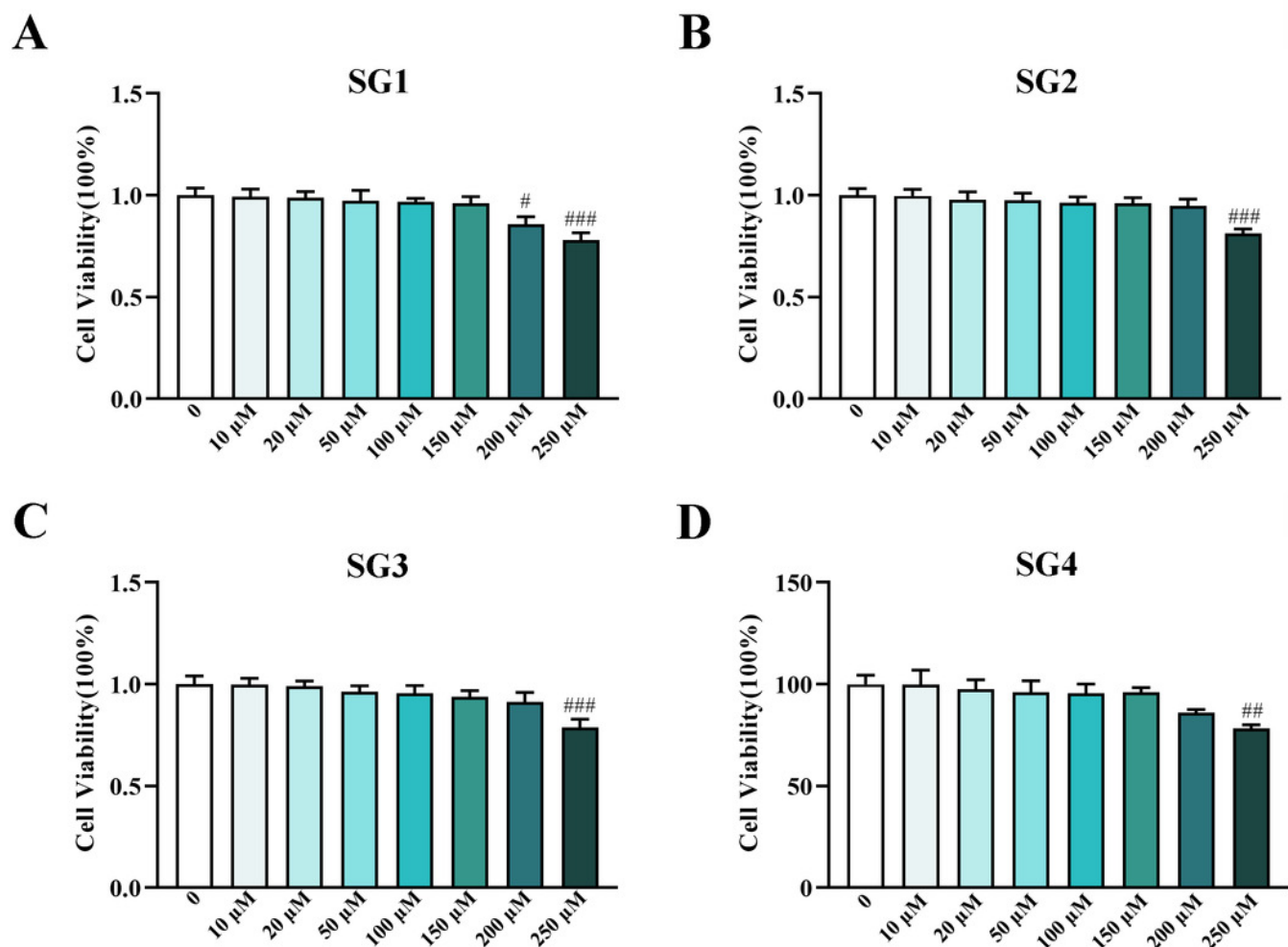
Figure 3

SGs on insulin-stimulated glucose uptake and lipid deposition in PA-treated HepG2 cells

SGs on insulin-stimulated glucose uptake and lipid deposition in PA-treated HepG2 cells. (A) Glucose uptake in HepG2 cells measured by 2-NBDG method ($n = 8$); (B) Oil Red O stain of HepG2 cells; (C and D) SGs treatment decreased TC and TG content in PA-treated HepG2 cells ($n = 8$). $^{##}P< 0.01$, $^{###}P< 0.001$ compared with control group; $^{*}P< 0.05$, $^{**}P < 0.01$, $^{***}P < 0.001$ compared with IR group.
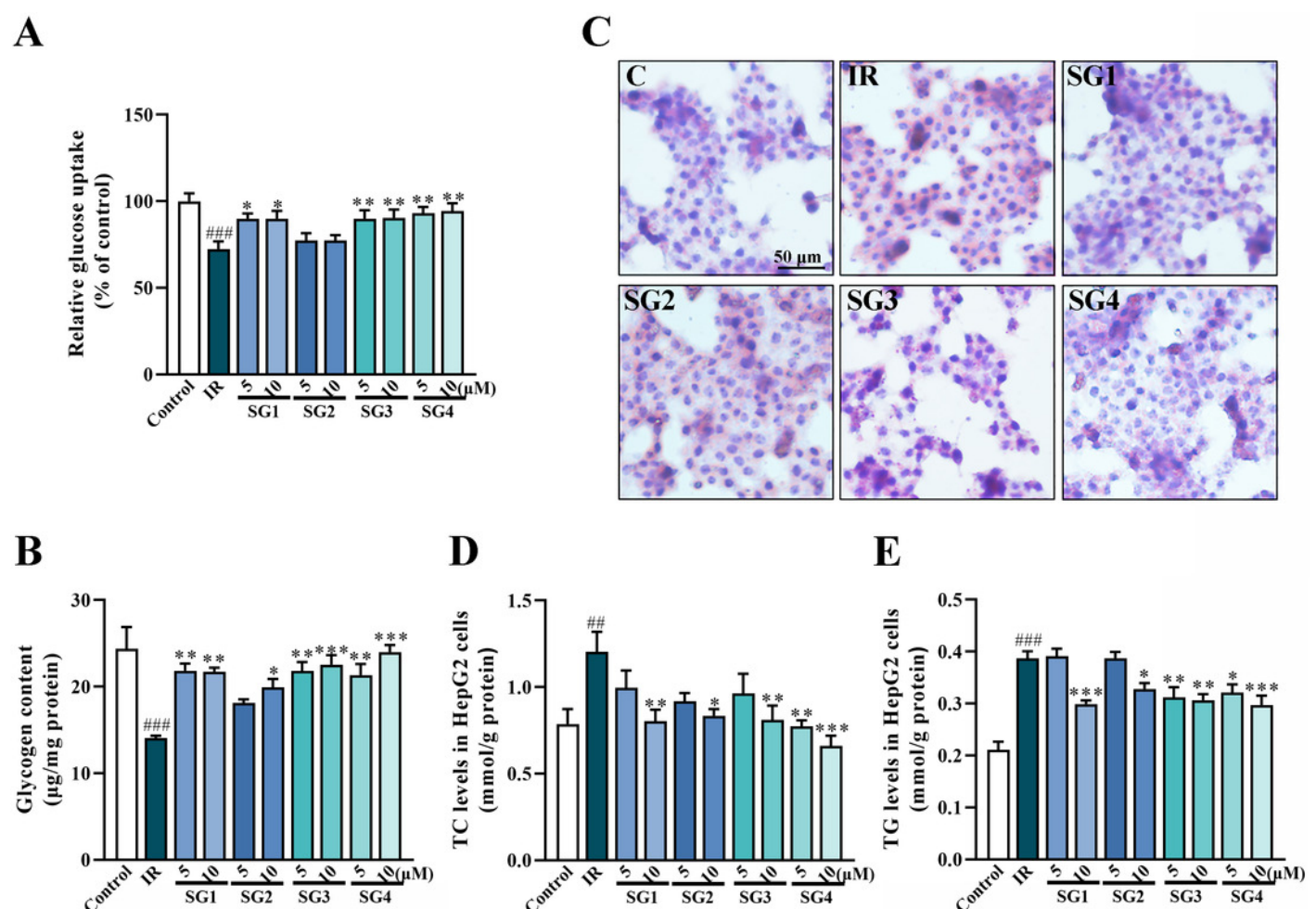
Figure 4

Western blot analysis of protein expression levels of AMPK signaling pathway

Western blot analysis of protein expression levels of AMPK signaling pathway. (A) Expression strips of all protein; (B) Phosphorylation level of AMPK normalized by AMPK , phosphorylation level of ACC normalized by ACC and phosphorylation level of IRS-1 normalized by IRS-1 (n = 3); (C) Phosphorylation level of Akt normalized by Akt (n = 3), SREBP-1 and FAS protein levels normalized by β-actin (n = 3). [##]P< 0.01 and [###]P< 0.001 compared with control group; [*]P< 0.05, [**]P < 0.01, [***]P < 0.001 compared with IR group.
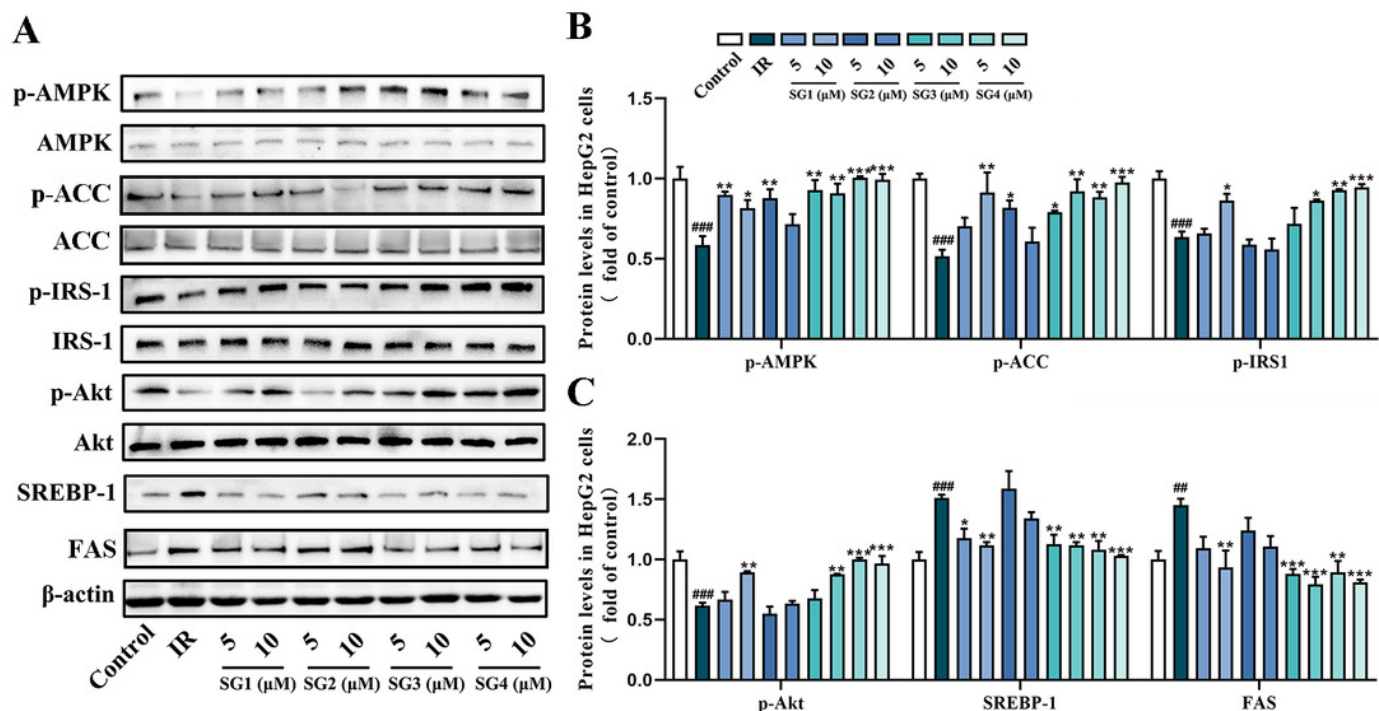
Figure 5

Western blot analysis of protein expression levels of AMPK signaling pathway after AICAR and CC treatment

Western blot analysis of protein expression levels of AMPK signaling pathway after AICAR and CC treatment. (A) Expression strips of the proteins of p-IRS1, IRS1, SREBP-1 and β-actin; (B) phosphorylation level of ACC normalized by ACC, phosphorylation level of IRS-1 normalized by IRS-1 and SREBP-1 protein level normalized by β-actin ($n = 3$) in HepG2 cells after AICAR treatment; (C) Expression strips of the proteins of p-ACC, ACC, p-IRS1, IRS1, SREBP-1 and β-actin; (D) phosphorylation level of ACC normalized by ACC, phosphorylation level of IRS-1 normalized by IRS-1 and SREBP-1 protein level normalized by β-actin ($n = 3$) in HepG2 cells after SGs and AICAR treatment. ###$P< 0.001$ compared with control group; *$P< 0.05$, **$P < 0.01$, ***$P < 0.001$ compared with IR group.